STRUCTURAL CHEMISTRY

Volume 76 (2020)

Supporting information for article:

Supramolecular networks supported by the anion···π linkage of Keggin-type heteropolyoxotungstates

Olha S. Panteleieva, Vira V. Ponomarova, Alexander V. Shtemenko and Kostiantyn V. Domasevitch

Index:

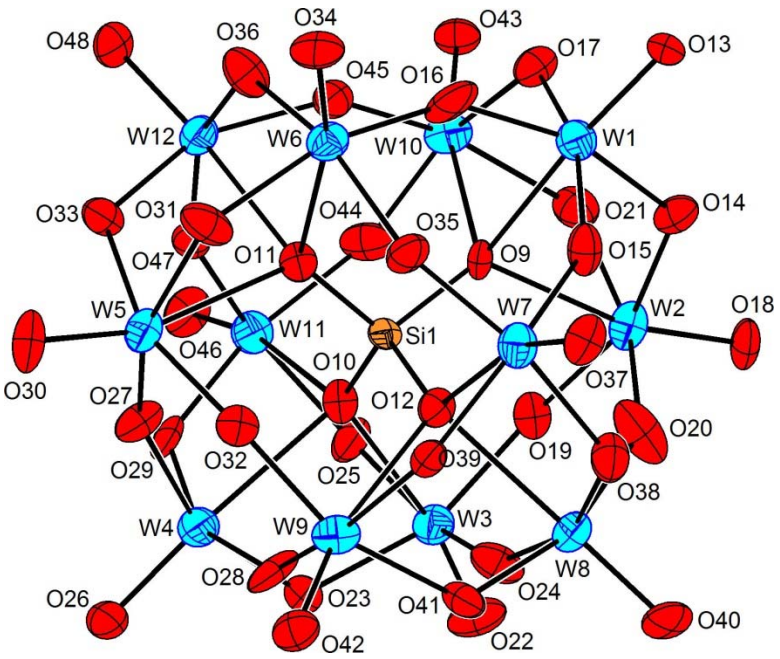

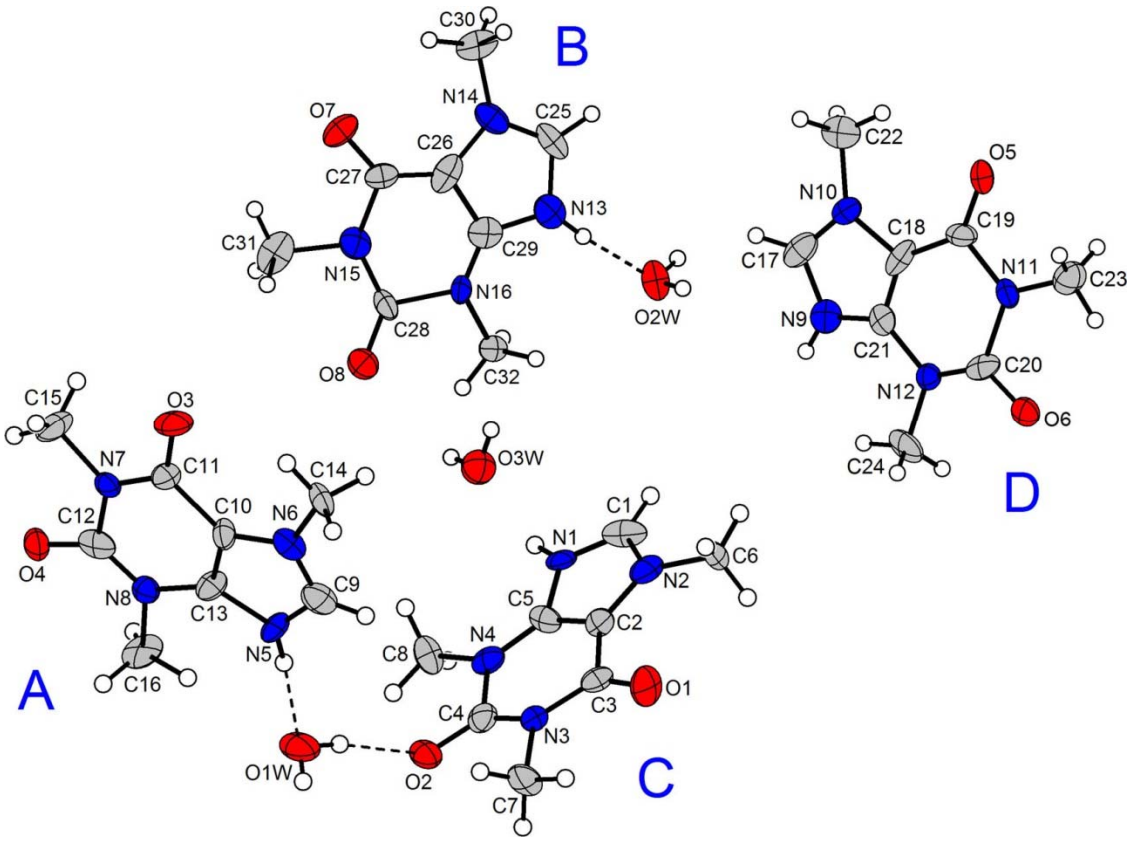

Fig. S1. Molecular structure of $(SiW_{12}O_{40})^{4-}$ anion (top) and caffeinium cations and solvent molecules in the crystal structure of $(HCaf)_4(SiW_{12}O_{40})\cdot 3H_2O$ (**1**), showing the atom labeling scheme. Thermal ellipsoids are drawn at 30% probability level and dotted lines indicate conventional hydrogen bonding. Atom O3W was refined isotropically.

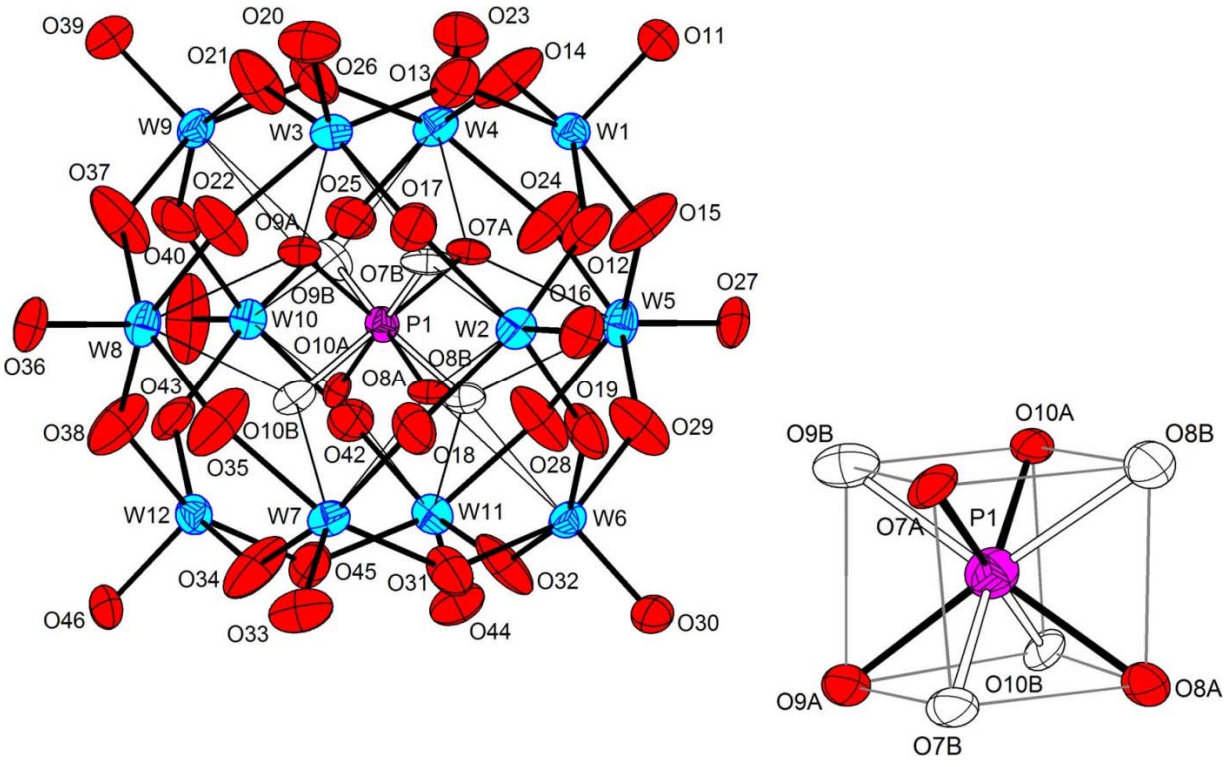

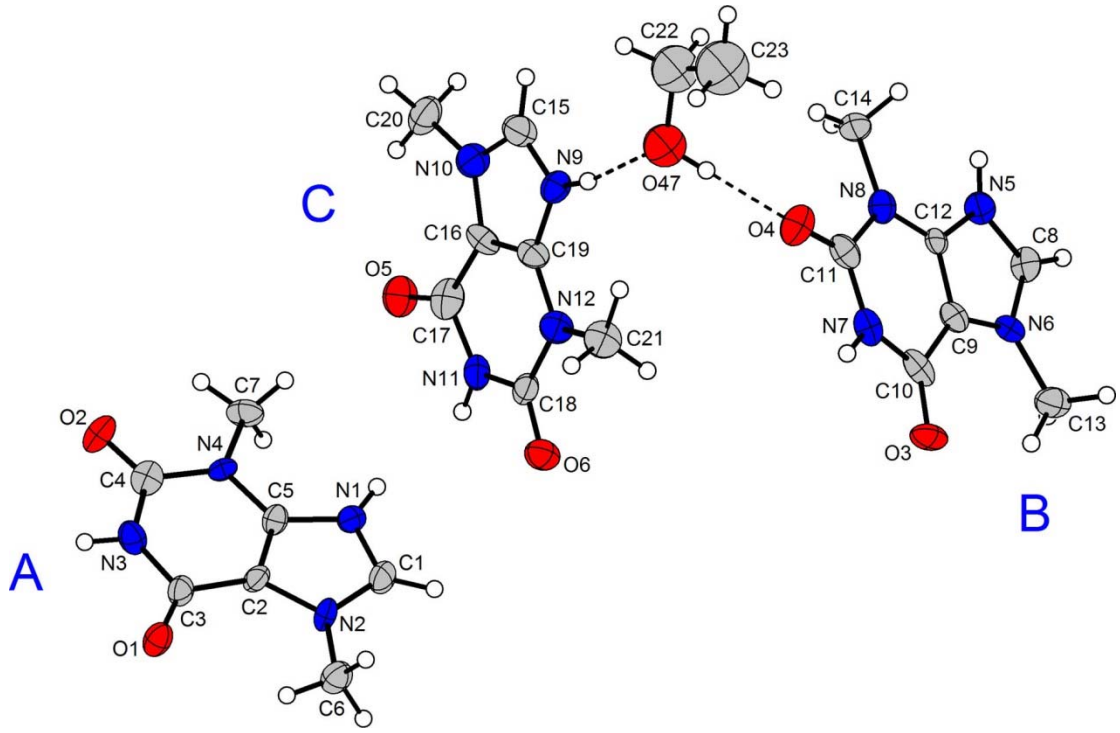

Fig. S2. Structure of $(HTbr)_3(PW_{12}O_{40})\cdot 1.5EtOH$ (2). Top: Molecular structure of $(PW_{12}O_{40})^{3-}$ anion, with thermal ellipsoids at 27% level, showing the atom labeling scheme and refined disordering scheme (50/50) for O-atoms of the central PO_4 tetrahedra. Bottom: theobrominium cations and solvent ethanol molecule in the crystal structure of (**2**), showing the atom labeling scheme. Thermal ellipsoids are drawn at 35% probability level and dotted lines indicate conventional hydrogen bonding. Atoms O47, O22, O23 were refined isotropically.

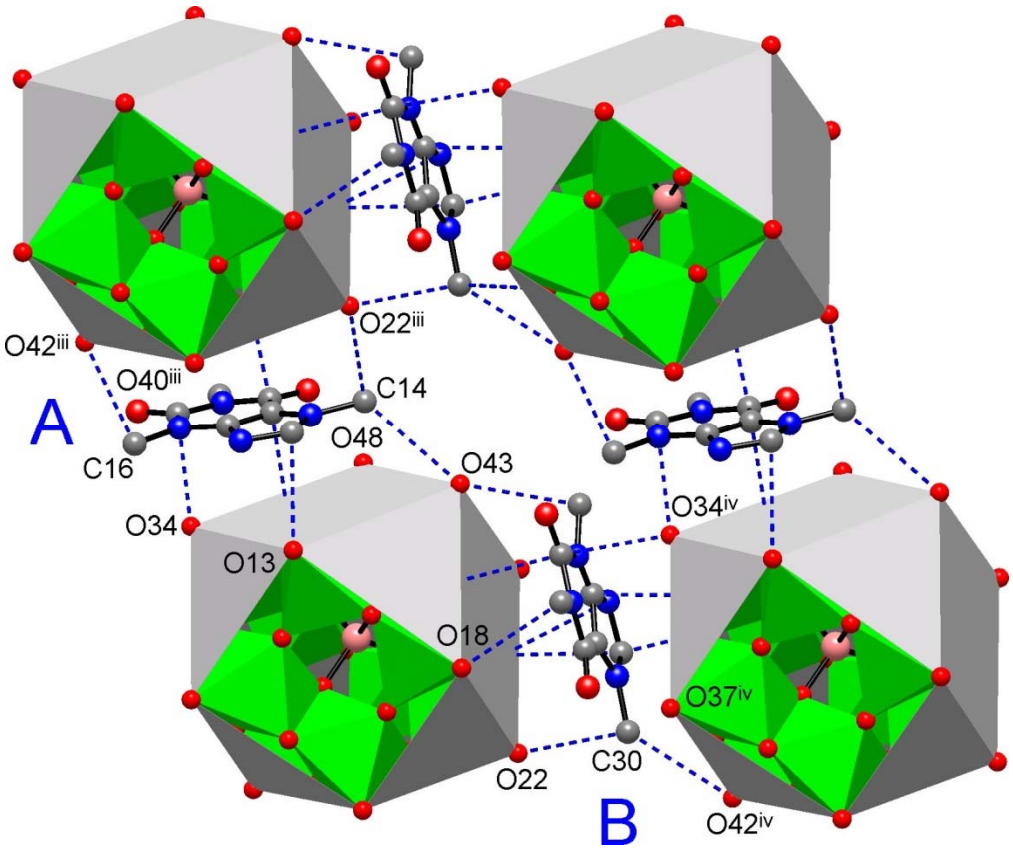

Fig. S3. Fragment of the square-grids network held by anion···π interactions in the crystal structure of $(HCaf)_4(SiW_{12}O_{40})\cdot 3H_2O$ (**1**), showing two unique caffeinium cations (A and B) sandwiched between pairs of $(SiW_{12}O_{40})^{3-}$ anions. Two other cations (C and D, See Fig. S1 for details) are terminal and they adopt stacking to only one anion. The anions are represented as grey cuboctahedra (defined by twelve terminal O-atoms) with open front faces. Blue dotted lines indicate set of short interactomic contacts of the types C···O and N···O (also involving C···O contacts of the methyl groups, which correspond to weak CH···O hydrogen bonding).

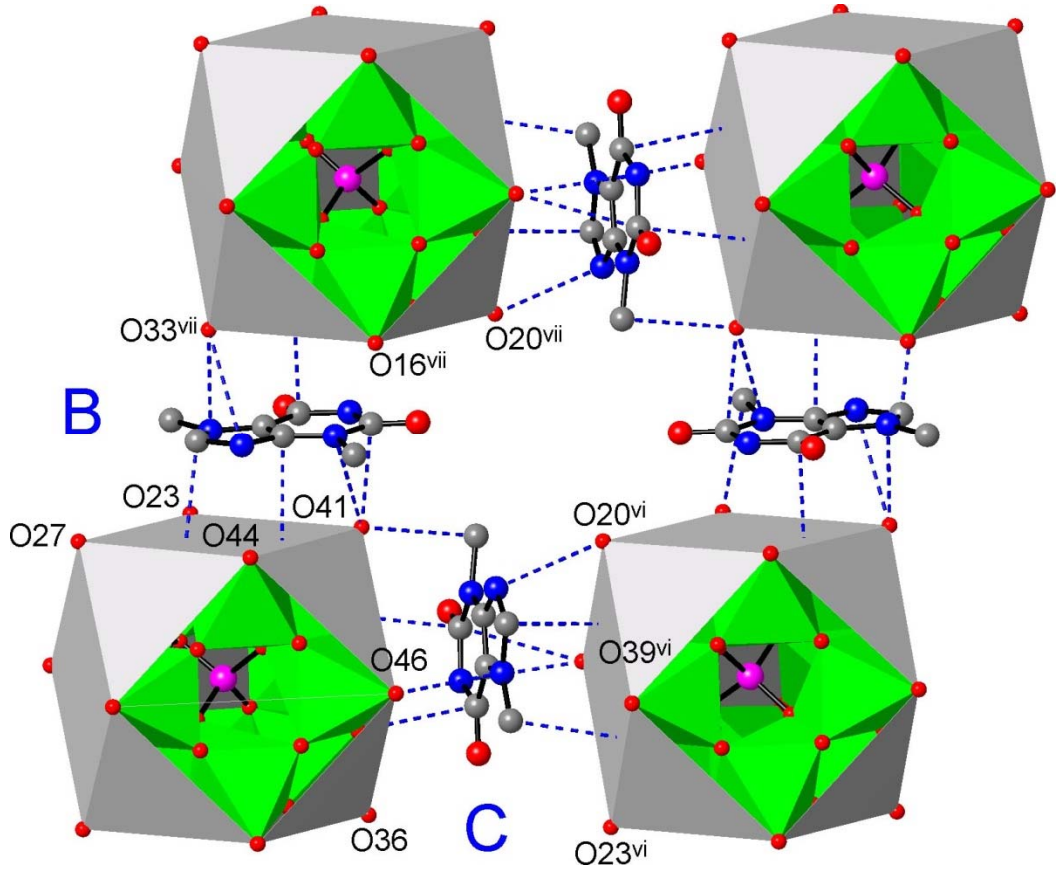

Fig. S4. Fragment of the square-grids network held by anion···π interactions in the crystal structure of $(HTbr)_3(PW_{12}O_{40})\cdot 1.5EtOH$ (2), showing two kinds of theobrominium cations (B and C) sandwiched between pairs of $(PW_{12}O_{40})^{3-}$ anions. The anions are represented as grey cuboctahedra (defined by twelve terminal O-atoms) with open front faces. Blue dotted lines indicate set of short interactomic contacts of the types C···O and N···O (also involving C···O contacts of the methyl groups, which correspond to weak CH···O hydrogen bonding).

[Symmetry codes: (vi) 1.5-x, 0.5+y, 0.5-z; (vii) -0.5+x, 0.5-y, -0.5+z.]

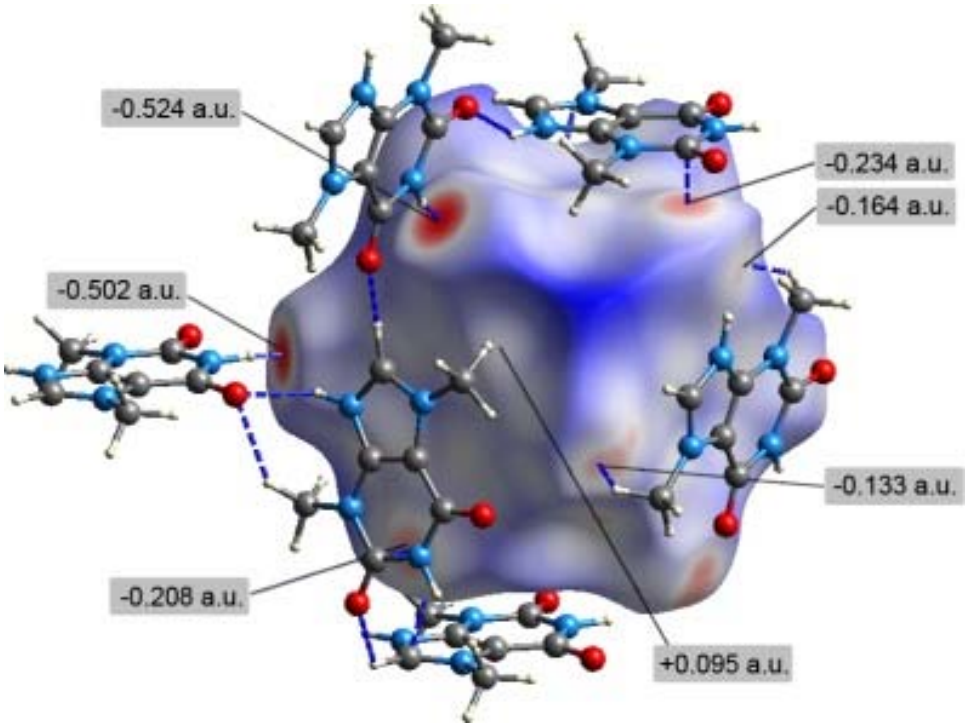

Fig. S5. The Hirshfeld surface of the $(PW_{12}O_{40})^{3-}$ anion in $(HTbr)_3(PW_{12}O_{40})\cdot 1.5EtOH$ (2) mapped over d_{norm} in the color range of -0.5673 (red) to 1.9522 a.u. (blue), with red spots indicating different kinds of interactions. Most prominent red spots correspond to strong conventional hydrogen bonding with amide donors of the cations. Weaker CH···O hydrogen bonding and anion···π interactions are also clearly visible on the surface.

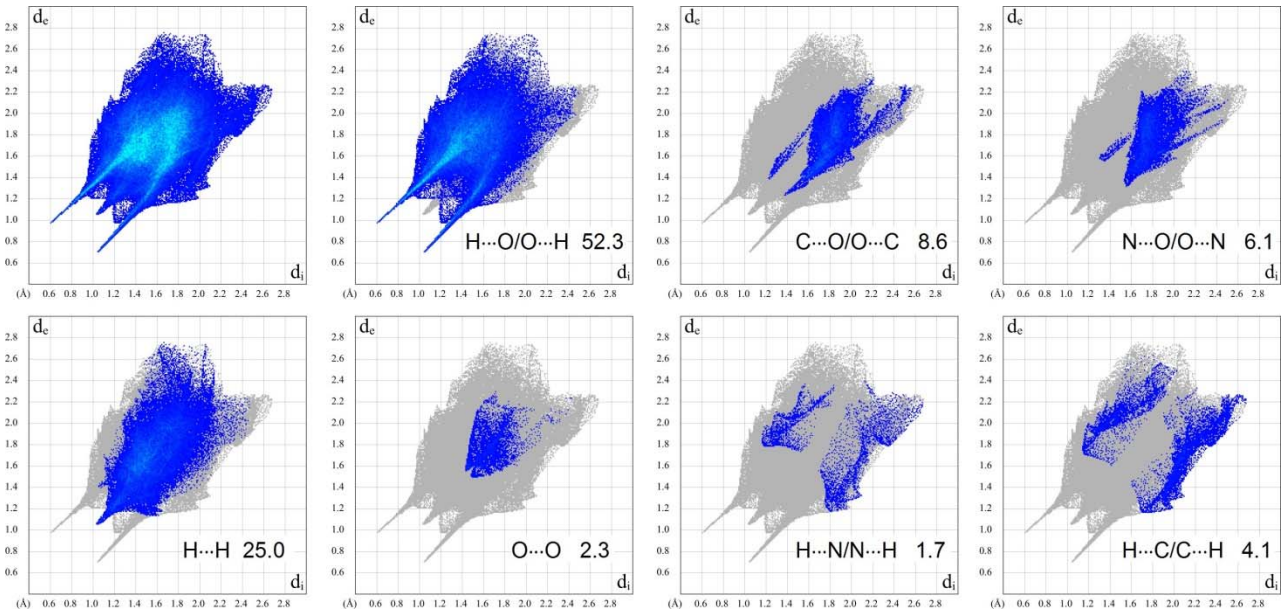

Fig. S6. Two-dimensional fingerprint plots for individual caffeinium cations in $(HCaf)_4(SiW_{12}O_{40})\cdot 3H_2O$ (1) (b), and delineated into the principal contributions (%) to the Hirshfeld surface from different kind of interatomic contacts. Note high contributions of C···O/O···C and N···O/O···N contacts (in total 14.7%), which correspond to the anion···π interactions between the cations and $(SiW_{12}O_{40})^{4-}$ anions.

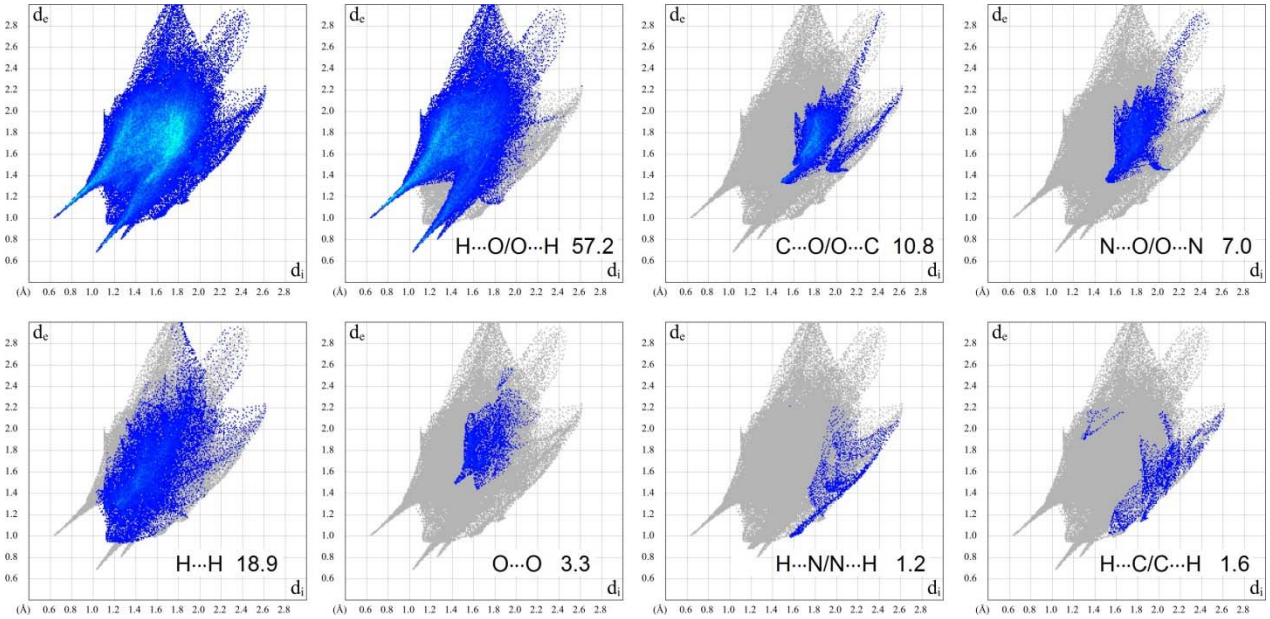

Fig. S7. Two-dimensional fingerprint plots for individual theobrominium cations in $(HTbr)_3(PW_{12}O_{40})\cdot 1.5EtOH$ (2), and delineated into the principal contributions (%) to the Hirshfeld surface from different kind of interatomic contacts.

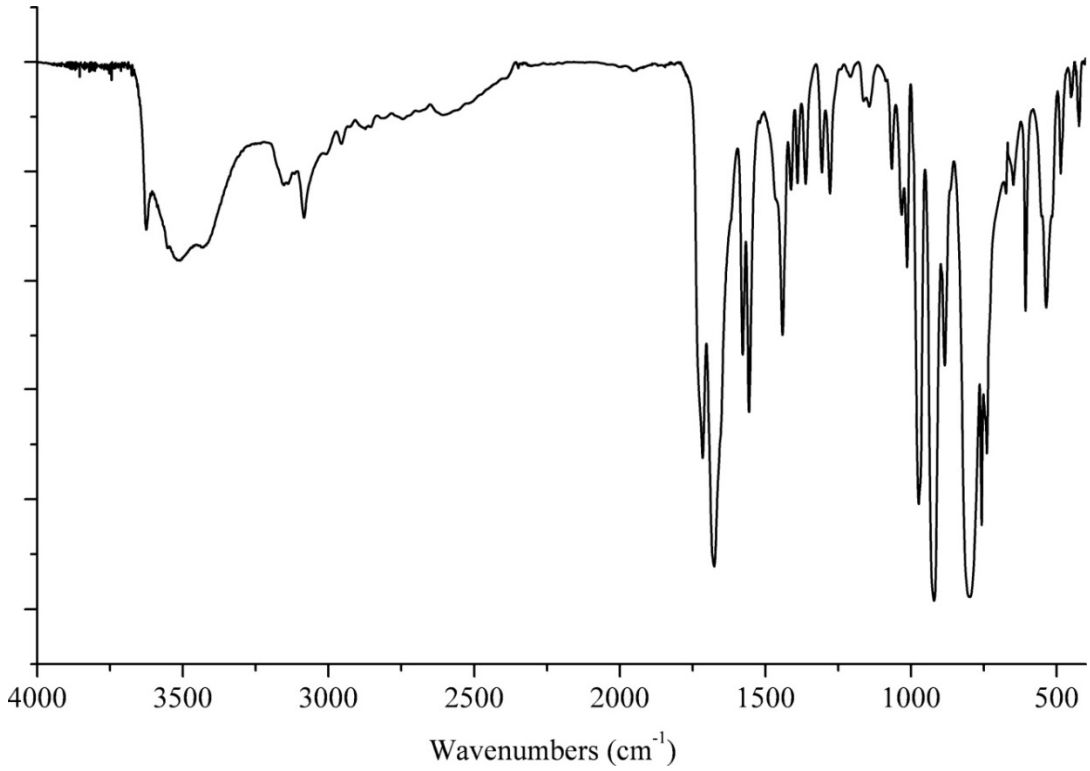

Fig. S8. IR spectrum of $(HCaf)_4(SiW_{12}O_{40})\cdot 3H_2O$ (**1**) (KBr discs, cm^{-1}).

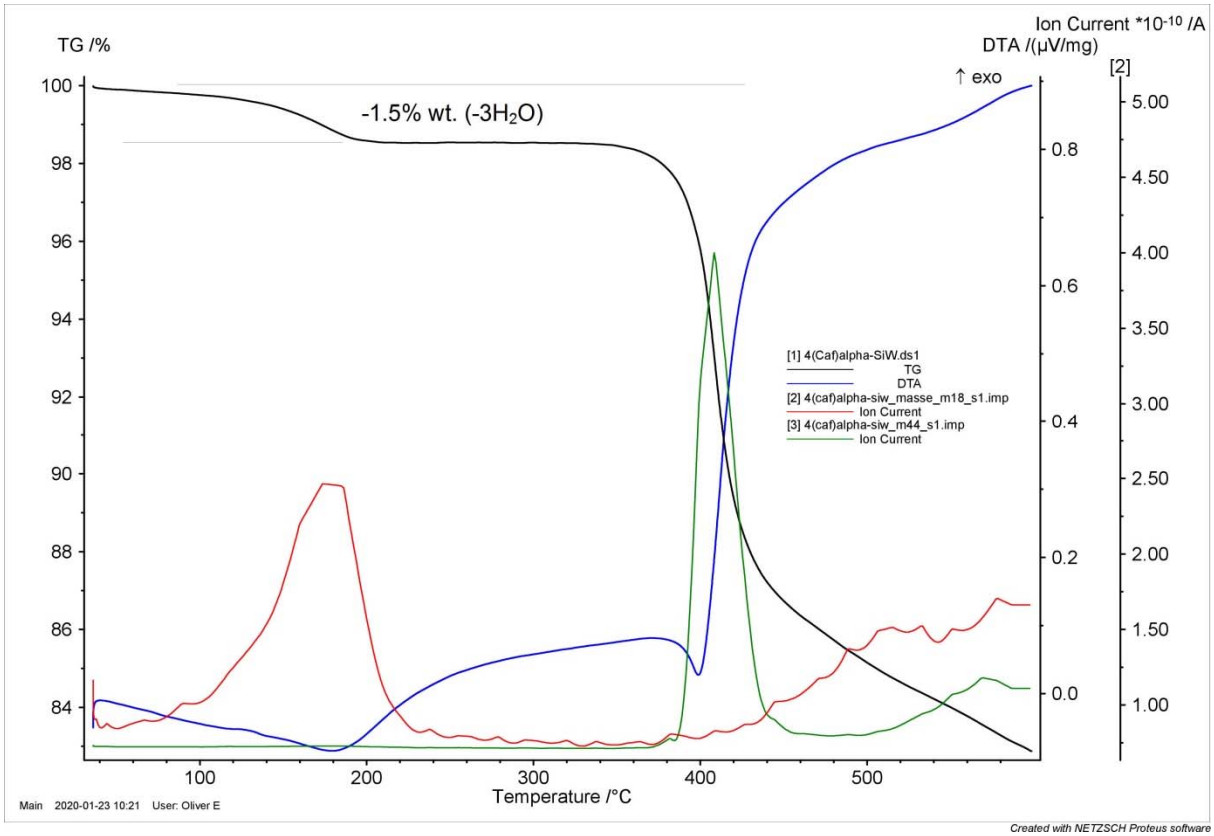

Fig. S9. TG/DTA plot for $(HCaf)_4(SiW_{12}O_{40})\cdot 3H_2O$ (1). Thermogravimetric/differential thermal analysis mass spectrometry (TG/DTA-MS) was performed on a Netzsch F1 Jupiter device connected to an Aeolos mass spectrometer. The sample was heated at a rate of 10 K min^{-1}.

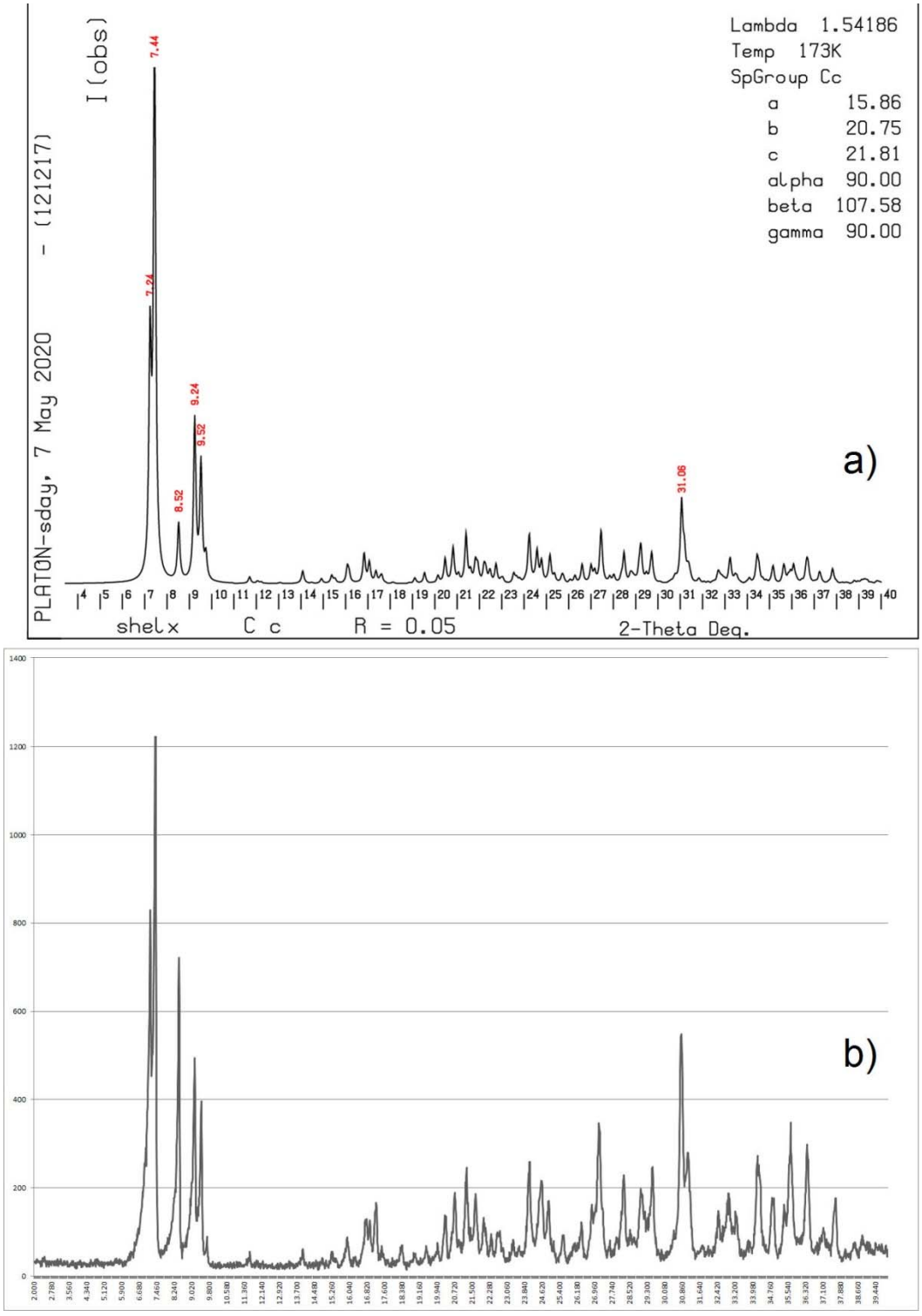

Fig S10. Simulated (a) and experimental (b) X-ray powder diffraction patterns for $(HCaf)_4(SiW_{12}O_{40})\cdot 3H_2O$ (1). PXRD analysis was carried out on a Stoe STADI-P (Cu $K\alpha_1$) using a linear PSD detector.

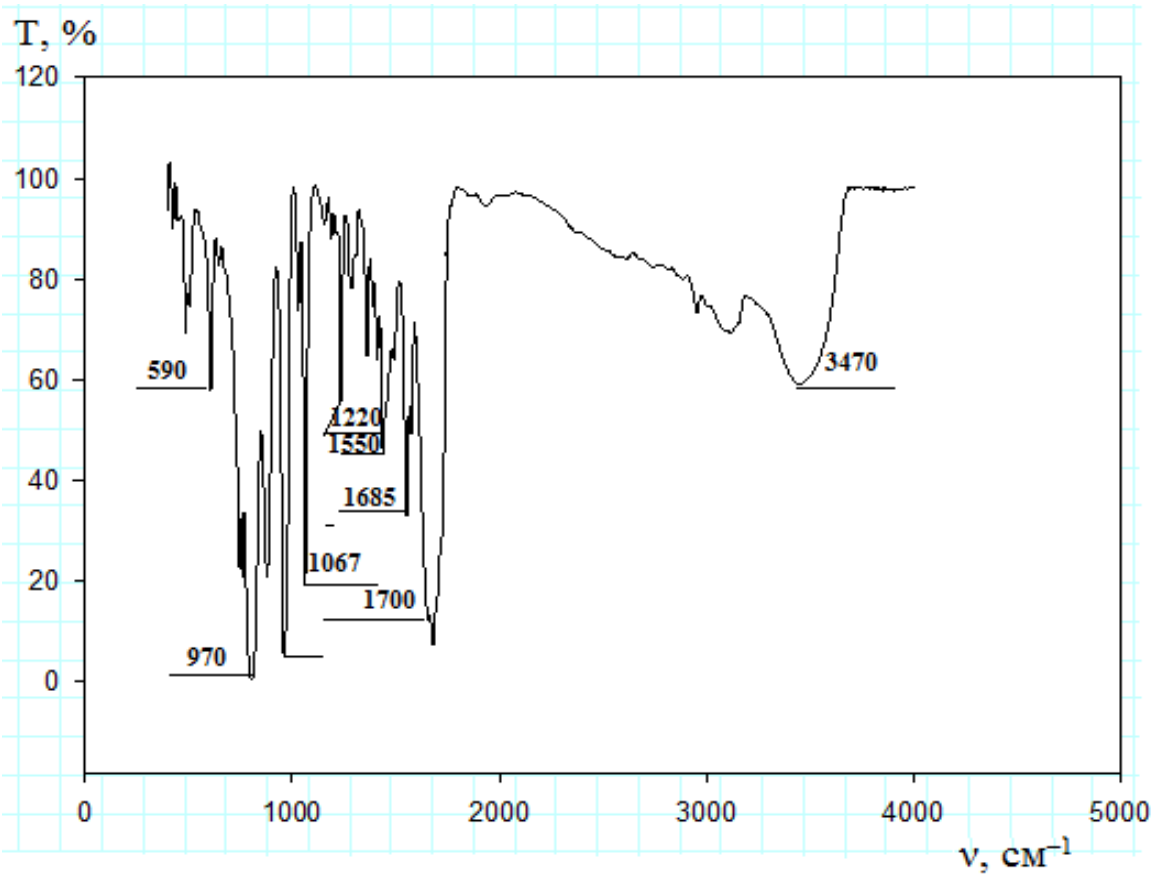

Fig. S11. IR spectrum of $(HTbr)_3(PW_{12}O_{40})\cdot 1.5EtOH$ (2) (KBr discs, cm^{-1}).

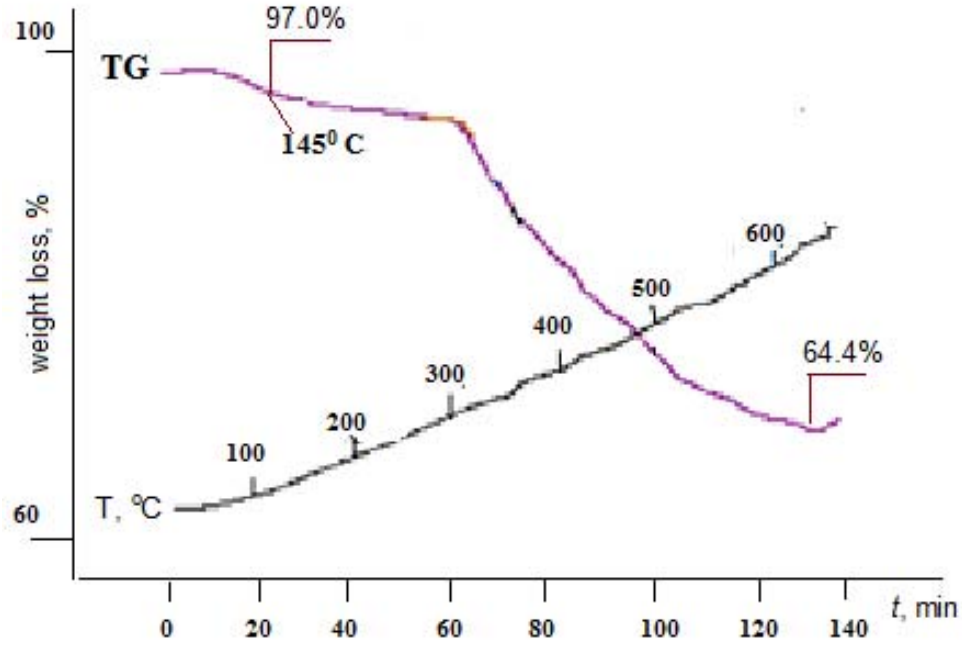

Fig. S12. TG plot for $(HTbr)_3(PW_{12}O_{40})\cdot 1.5EtOH$ (2). Thermogravimetric thermal analysis was performed on a derivatograph of "Paulik-Paulik-Erdei" system. The sample was heated at a rate of 5 K min^{-1}.

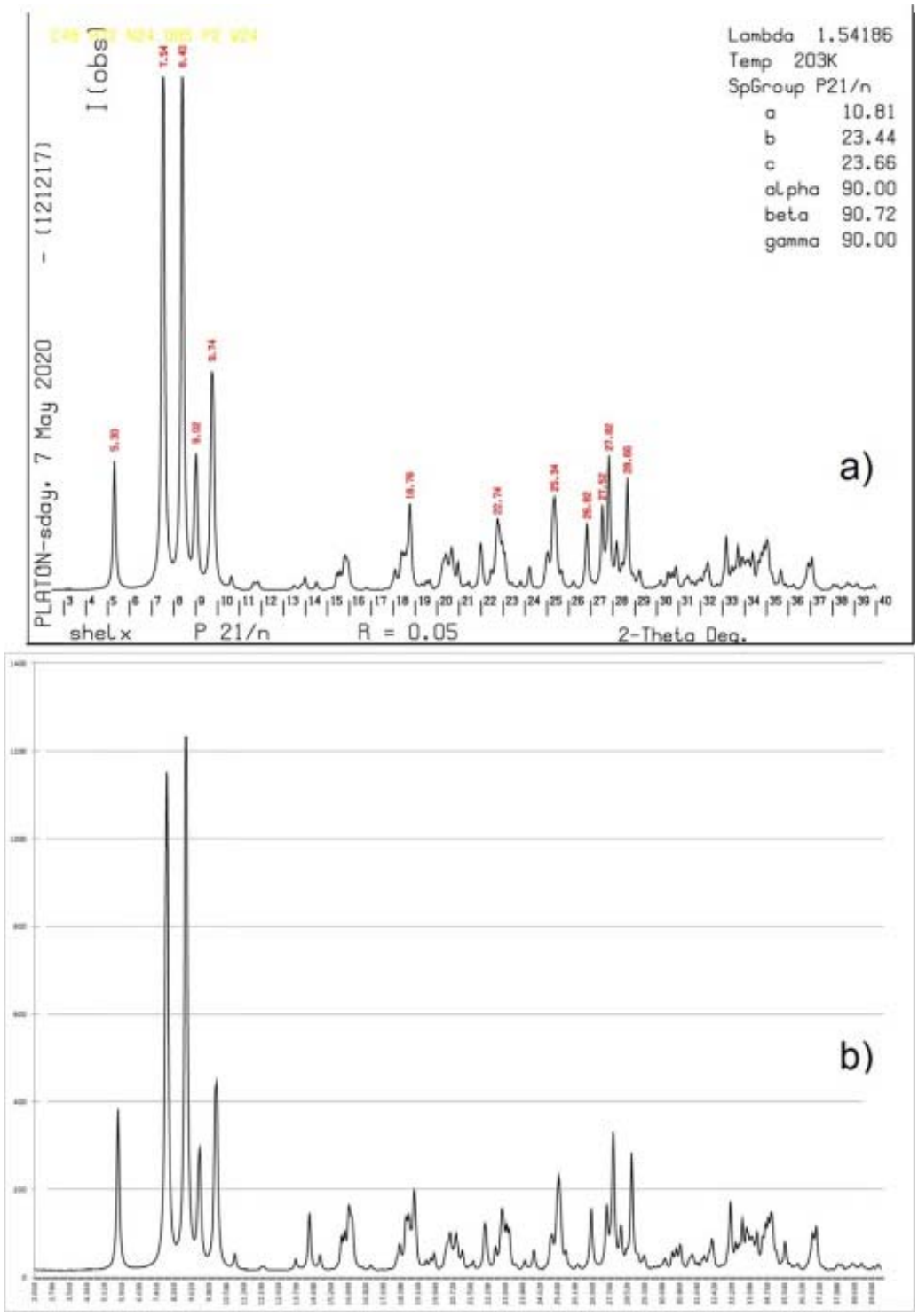

Fig S13. Simulated (a) and experimental (b) X-ray powder diffraction patterns for $(HTbr)_3(PW_{12}O_{40})\cdot 1.5EtOH$ (2). PXRD analysis was carried out on a Shimadzu XRD-6000 (Cu Kα-radiation).